Accepted Manuscript

Mechanical modeling of collective cell migration: An agent-based and continuum material approach

Ismael González-Valverde, José Manuel García-Aznar

PII: S0045-7825(18)30160-9
DOI: https://doi.org/10.1016/j.cma.2018.03.036
Reference: CMA 11842

To appear in: *Comput. Methods Appl. Mech. Engrg.*

Received date : 10 November 2017
Revised date : 20 March 2018
Accepted date : 25 March 2018

Please cite this article as: I. González-Valverde, J.M. García-Aznar, Mechanical modeling of collective cell migration: An agent-based and continuum material approach, *Comput. Methods Appl. Mech. Engrg.* (2018), https://doi.org/10.1016/j.cma.2018.03.036

***Highlights (for review)**

- We simulate epithelial layer mechanics combining a discrete agent-based model and a continuum material model.
- We use a hybrid representation of individual cells as particles and polygons.
- We model an epithelial layer as a continuum medium with different domains.
- We simulate two common examples of cell collective migration: durotaxis and gap closure.

Mechanical Modeling of Collective Cell Migration: An Agent-based and Continuum Material Approach

Ismael González-Valverde[1], José Manuel García-Aznar[1]*

[1] M2BE, Department of Mechanical Engineering, Aragon Institute of Engineering Research (I3A), University of Zaragoza, Zaragoza, Spain

*Corresponding author: jmgaraz@unizar.es

Abstract

We develop a novel modeling approach that combines a discrete agent-based model and a continuum material model to simulate collective cell migration in epithelial layers. In this approach, cells are represented as particles located at their geometrical center, but also as a polygonal body derived from the Voronoi diagram. Furthermore, we model the tissue as a continuum medium with different spatial domains that represent cell and substrate materials. In fact, the mechanical behavior of each domain is affected by the presence of cells from the discrete model. Moreover, we solve this mechanical problem using the finite element method (FEM). The forces generated by cells are projected to the FE mesh, that is created dynamically during the simulation from the discrete cell representation. After the FE resolution, we use the mesh displacements to determine the new cell positions in the agent-based model. Finally, to demonstrate the potential of this approach to model epithelial tissue mechanics, we simulate two well-studied cases of collective cell migration: durotaxis and gap closure. We use the experimental data from the literature to validate our numerical results. Therefore, the modeling strategy here presented offers a new perspective for a deeper understanding of tissue mechanics that emerge from cell dynamics in epithelial layers.

Keywords: cell mechanics, finite element method, agent-based, particle modeling, gap closure, durotaxis

1 Introduction

The mechanical modeling of collective cell migration in epithelial tissues is a complex task since many biophysical phenomena occur simultaneously. First, the interaction forces between cells and with the extra-cellular matrix need to be modeled [1–4]. In addition, cell and substrate mechanical properties also affect the system mechanical behavior [4–7]. Moreover, the tissue morphology suffers considerable changes in these biological processes due to cell proliferation, cell rearrangements, and cell shape changes [8]. Finally, to study cell collective behavior and observe the effects at the tissue level, we need to have a reasonable number of cells in the simulations.

Previous works on modeling collective migration have engaged this biological problem using very different approaches. We find many models focused on simulating cells as individual units in the tissue [9,10]. First, center-based and simple particle models offer a straightforward way to track cell information and to calculate their interactions [11–13]. However, these methods hardly represent tissue morphology and cell shapes inside a monolayer. Vertex-based model is another common modeling strategy to simulate epithelial tissues, and they overcome some limitations of the former type of models [14–16]. For instance, cell representation is more accurate and cell-cell interfaces are clearly defined. Nonetheless, they are not free of disadvantages. Cell rearrangements and cell proliferation need to be considered carefully and transitions of cell number of vertices and neighboring must be explicitly handled. In recent years, we also find an interesting combination of center-based and vertex-based models that extend the modeling capabilities of both approaches [17–19]. Recently, some authors are focusing their efforts on developing 3D deformable cells systems [20,21]. Nevertheless, they are still very computationally expensive and complicated to apply to biomechanical processes with many cells. In contrast, Potts models are very flexible and usually very efficient even simulating a high number of cells [22,23]. They are often considered to be excessively phenomenological by many authors but, in fact, they have been successfully applied to model cell and tissue mechanical behavior. Furthermore, sub-cellular and molecular-based models have been used to describe the basis of collective migration in epithelial layers [4,24,25]. These models are especially useful to simulate and study very specific molecular mechanisms. However, they are limited to simulate only a few cells and not many simultaneous biological processes.

Differently, other researchers focus on the opposite approach, and they reproduce multi-cellular systems using continuum models [26–29]. For example, epithelial tissue migration can be modeled as a continuum medium and the mechanical problem solved using the finite element method (FEM) [27–29]. This type of model scales very well for large cell layers but, unfortunately, they do not consider the geometry and behavior of individual cells in the tissue. In addition, some biophysical phenomena are difficult to integrate into this modeling approach.

In this work, we propose a modeling approach that combines an agent-based model and a continuum material model to simulate the mechanical behavior of cells in epithelial tissues. Further, we focus on

designing a flexible geometrical representation of the cells and a modular force generation system. In fact, we take some ideas of vertex-based models combined with center-based particle models to represent cells in our modeling approach. Cells are described as discrete particles but they also have a polygonal body associated, that is generated using the Voronoi diagram. In contrast, we model the whole tissue as a continuum media with different domains, basically, cell and substrate domains. The domain properties are defined by the presence of cells and the forces they generate. To solve this mechanical problem, we rely on the finite element method. Therefore, we aim to explore the possibilities that the combination of cell-based models with finite element method can bring to epithelial mechanics modeling since this approach has not been explored in detail previously. In addition, we present two examples of application of our approach, and we compare them with experimental data taken from previous works of other authors [4,27,30]. These examples are based on two extensively studied collective migration processes: durotaxis and gap closure.

2 Methods

Our modeling approach is based on three fundamental aspects that are described in Figure 1: a discrete cell model, a continuum material model and the interfaces between them. The connection between both models is driven by an adaptable geometry module and several cell force models.

First, we use a discrete cell model in order to track the individual cell information in the tissue. In this way, we are able to characterize individually cell behavior and the direct interaction between each cell and its neighbors and with the substrate. Second, we rely on a continuum material model to create an approximation at the tissue level mechanics. This assumption is supported by the fact that cells in the epithelial tissue are tightly connected by cell-cell junctions [7]. Hence, epithelial monolayer can behave as a continuum media, and some of their mechanical properties can be characterized experimentally [5]. In our continuum material model, we can define several spatial domains in the monolayer and assign them different properties. Moreover, we can specify precise mechanical boundary conditions on our simulations using this continuum approach.

Lastly, to connect both models, we use some geometrical techniques that ease the transition between continuum and discrete representations of cells in the tissue. To tackle cell morphology changes and rearrangements in the monolayer, we must be capable of adapting our representation dynamically to new shapes. To achieve this goal, we combine different tessellation, shape reconstruction and mesh refinement methods. Furthermore, we use several force models based on biophysical phenomena to describe cell behavior in the monolayer.

Figure 1. Conceptual diagram of the modeling approach. Discrete cell model provides information to geometry and force generation modules. Additionally, to generate the forces used in this approach, forces module also relies on the geometrical representation of the cells. The continuum material model works with the output of geometrical and force modules. Finally, the information generated in the continuum material model is fed back to the discrete cell model.

2.1 Discrete cell model

In our modeling approach, we represent each cell of the tissue as a discrete unit. We use an agent-based approach to independently model every cell. Basically, each cell i is defined as a discrete entity $S_i^{cell}(\boldsymbol{p_i}, R_i, \tau_i)$, whose centroid position is represented by the vector $\boldsymbol{p_i}$. Every cell has associated a particle virtual radius denoted by R_i and an internal clock denoted by τ_i. The set of all the cells is denoted by $S^{cell} = \{S_1^{cell}, S_2^{cell}, \ldots, S_n^{cell}\}$. Therefore, we are able to keep separated the cell information for each unit and associate independent biophysical processes to them, for instance, its life cycle. In addition, we can track cell position, trajectories and distance traveled directly.

To model cell life cycle, we assume that cells are exclusively in a proliferative state or quiescent. In other words, they can be in an active state of their cycle, that ends up on cell division or, otherwise, in a resting state. We consider that the proliferative state represents both the interphase and the mitotic phase as a simplification of the actual biological process. As shown in equation (1), cell internal clock state (τ_i) is incremented in each time step (Δt) if its value is under the cycle division threshold (θ^{cycle}). This process is also regulated by a growing speed parameter (λ^{cycle}). After a cycle is completed, a new daughter cell is generated near its parent cell and both restart their life cycles independently (see Figure S01). The duration of the process until cell divides has a slight variability – normal distribution *N* – to avoid any clustering effect.

Equation (1)
$$\begin{aligned} &if\ \tau_i(t) < \theta^{cycle} \quad \Rightarrow \quad \tau_i(t+\Delta t) = \tau_i(t) + \lambda^{cycle} \cdot \Delta t \\ &if\ \tau_i(t) > \theta^{cycle} \quad \Rightarrow \quad \tau_i(t+\Delta t) = N\left(mean = 0.2 \cdot \theta^{cycle}, dev = 0.1 \cdot \theta^{cycle}\right) \end{aligned}$$

This discrete particle-based model is a central part of this work but its cell representation is rather limited. To extend the simulation capabilities of our approach, we generate a more elaborated cell geometry using the information provided by this model as it is described in the following sections. Additionally, the generation of forces depends on some information managed by the discrete model but also on the extended geometrical representation. Hence, the modeling of the forces is tightly related to the discrete model but it can be considered separated from it.

2.2 Continuum material model

In contrast to the discrete cell model, our continuum material model represents the mechanical behavior at the tissue level. In fact, it is focused on modeling the passive mechanics of the tissue and its properties as a continuum solid [5]. Basically, we consider that tissue can be divided into a cell material (Ω_{cell}) or a substrate material($\Omega_{substrate}$) considering if cells are present or not. In addition, we define the interface between these materials by $\Gamma^{cell-substrate}$.

We assume that the force equilibrium in the cell domain is given by cell material stress ($\boldsymbol{\sigma}^{cell}$) and the forces generated by cells ($\boldsymbol{F}^{cell}$), that will be described in detail later in section 2.4. On the other hand, we do not consider additional forces in the substrate domain, just the substrate material stresses ($\boldsymbol{\sigma}^{substrate}$). Finally, cell and substrate material stresses must be in equilibrium in the interface $\Gamma^{cell-substrate}$. These equilibrium equations are described as follows:

Equation (2A) $\nabla \cdot (\boldsymbol{\sigma}^{cell}) + \boldsymbol{F}^{cell} = \mathbf{0}$ in Ω_{cell}

Equation (2B) $\nabla \cdot (\boldsymbol{\sigma}^{substrate}) = \mathbf{0}$ in $\Omega_{substrate}$

Equation (2C) $\boldsymbol{\sigma}^{cell} = \boldsymbol{\sigma}^{substrate}$ in $\Gamma^{cell-substrate}$

Furthermore, we define a constitutive law for the different materials that can be present in the tissue as shown in equation (3A). Hence, these materials are separated into independent domains with different mechanical properties ($\boldsymbol{C}^{\Omega_n}$), and they interact through their interfaces. In this paper, we assume that cell material ($\boldsymbol{C}^{\Omega_{cell}}$) possesses constant properties, but substrate material stiffness ($\boldsymbol{C}^{\Omega_{substrate}}$) may depend on spatial coordinates ($\boldsymbol{x}$) as illustrated in equation (3C). This model facilitates the simulation of stiffness gradients in the substrate, that is fundamental to analyze biophysical phenomena such as durotaxis. The stiffness gradient slope is defined by $m(\boldsymbol{x})$, the second-order identity tensor by **1,** the fourth-order identity tensor by $\boldsymbol{I}$ and the stress and strain tensors by $\boldsymbol{\sigma}$ and $\boldsymbol{\varepsilon}$, respectively. In addition, we define the mechanical properties of the *n* domain: λ^{Ω_n} as the first Lamé parameter, G^{Ω_n} as the shear modulus, ν^{Ω_n} as Poisson's ratio and E^{Ω_n} as Young's modulus.

Equation (3A)

$$\boldsymbol{\sigma}=\boldsymbol{C}^{\Omega_n}:\boldsymbol{\varepsilon} \qquad for \quad n=[substrate, cell]$$

$$\boldsymbol{C}^{\Omega_n}=\lambda^{\Omega_n}\mathbf{1}\otimes\mathbf{1}+G^{\Omega_n}\boldsymbol{I}=\frac{\nu_{PSH}^{\Omega_n}}{(1+\nu_{PSH}^{\Omega_n})+(1-2\,\nu_{PSH}^{\Omega_n})}E_{PSH}^{\Omega_n}\mathbf{1}\otimes\mathbf{1}+\frac{1}{2(1+\nu_{PSH}^{\Omega_n})}E_{PSH}^{\Omega_n}\boldsymbol{I}$$

Equation (3B)

$$\nu_{PSH}^{\Omega_n}=\frac{\nu^{\Omega_n}}{1-\nu^{\Omega_n}}$$

$$E_{PSH}^{\Omega_n}=\frac{E^{\Omega_n}}{1-(\nu^{\Omega_n})^2}$$

Equation (3C)

$$E^{\Omega_{substrate}}(\boldsymbol{x})=E^{substrate}+m(\boldsymbol{x}) \qquad for \quad \boldsymbol{x}\in\mathbb{R}^2$$

$$E^{\Omega_{cell}}=E^{cell}\neq E(\boldsymbol{x})$$

We use the finite element method (FEM) to solve the continuum mechanical problem at the tissue level. Each domain considered in the model is represented by independent elements of the FE mesh. To connect these separated domains, we use coincident nodes in their interfaces. Moreover, in order to solve the system in 2D, we assume the plane stress hypothesis (PSH) since one of the monolayer dimensions (thickness) is very small compared to the others. We transform the material parameters as shown in equation (3B).

Mesh and force generation are explained in detail in their corresponding sections but it is worth noting here their implications in the continuum model. In particular, the mesh used for the FE resolution is generated using cell centroids of the discrete model and the additional polygonal representation of cell bodies. Furthermore, the cell forces are applied to nodes that correspond to either the cell vertices or centroids used to generate the mesh. Hence, these two aspects of our approach are the actual connection between discrete and continuum models.

Finally, after solving the FE problem, we use the deformed mesh to obtain cell displacements from the nodes that represent the cell centroids. These displacements are processed by the discrete model to update cell positions.

2.3 Adaptable geometry

Since tissue morphology changes during cell reorganization, proliferation and migration processes, we need to use a cell geometrical representation flexible enough to adapt to these alterations. Discrete particle model offers a rather limited representation of the cell body. However, we extend cell geometry from a discrete point to a polygon using a Voronoi diagram built from cell centroids. Furthermore, to define the tissue domains, we create alpha shapes that depend on the cell distribution. Lastly, FE mesh is generated using information of the Voronoi diagram and the alpha shapes. Using all these techniques, we effectively connect discrete and continuum models at the geometrical level.

Figure 2. Geometry generation. (A) We generate the Voronoi diagram V^{cell} from cell centroids S^{cell} of the discrete model. (B) We create the alpha shapes S^{α} from the virtual circles U^{cell} centered on cell centroids S^{cell}. We use the alpha shapes to differentiate cell domain Ω_{cell} from substrate domain $\Omega_{substrate}$ and, therefore, to define the limits of the epithelial monolayer. (C) We generate the FE mesh (M^{FEM}) from a Delaunay triangulation of the following set of points: cell centroids (S^{cell}), cell vertices (V^{cell}), alpha shapes (S^{α}) and a regular grid in the substrate domain (S^{grid}).

Voronoi diagram

We use the Voronoi diagram to generate a representation of cell body using the information from our discrete model (S^{cell}). This tessellation technique divides the plane using an initial set of points into regions (V_i^{cell}) whose distance to its generator point (S_i^{cell}) is less than to any other initial point (S_j^{cell}) as shown in equation (4). The resultant convex polygon V_i^{cell} represents the cell body associated to each cell centroid S_i^{cell} as it is shown in Figure 2A. We use the function $d(\boldsymbol{x}, \boldsymbol{p_i})$ to describe the distance between a point ($\boldsymbol{x}$) and the cell centroid position ($\boldsymbol{p_i}$).

Equation (4) $$V_i^{cell} = \{\boldsymbol{x} \in \mathbb{R}^2 \ : \ d(\boldsymbol{x}, \boldsymbol{p_i}) < d(\boldsymbol{x}, \boldsymbol{p_j}) \quad for \quad i \neq j\}$$

In fact, this cell representation is fundamental to join both continuum and discrete models together. We create a transition from a pure discrete particle-based representation of cells to a partitioned continuum space. In our approach, this tessellation is generated dynamically, in other words, it is a stateless representation of the cell body that it is not stored from one step to the next. It can also be described as a transient vertex-based model since we use this polygonal body to simulate more detailed cell

behavior and to map forces. Additionally, the Voronoi diagram is a reliable tool to determine neighboring and shared edges between cells in the monolayer ($S_i^{neighbors} \subset S^{cells}$).

Last, we use this polygonal representation to determine daughter cell position after cell division. We calculate the minimum ellipse that contains the polygon and force the cell cleavage on the minor axis of that ellipse (see Figure S1).

Alpha shapes

To differentiate between distinct tissue domains, we generate alpha shapes from our discrete model. These are a family of linear curves associated to a set of points, in our case, to the cells. Alpha shapes are defined by an α parameter that is related to the maximum distance between points for connecting them. In the case of $\alpha \to \infty$, the curve obtained contains all considered points. On the contrary, when $\alpha \to 0$, alpha shapes just degenerates to the set of points. Moreover, more than one curve can be created using this technique. It is even possible to generate '*holes*' inside closed curves.

Instead of generating alpha shapes only from cell centroids (S^{cell}), we use virtual circles (U^{cell}) centered on each centroid as shown in equation (5) and Figure 2B. The virtual circle associated to each cell (U_i^{cell}) is defined by the virtual cell radius (R_i), that it is also used for the cell-cell interactions as it is explained later on this paper. In this way, we are able to represent the body of cells located in the monolayer boundary or completely isolated. Hence, we avoid a collapse of the alpha shape to the cell centroid.

Equation (5) $S^{\alpha} = f(U^{cell}, \alpha)$

We define $f(S, \alpha)$ as the function that generates all possible alpha shapes and S^{α} as the alpha shape for our current set of points for a given α value.

Finally, since Voronoi diagram is a tessellation of an infinite plane by definition, we use these alpha shapes in order to limit the polygonal representation to a finite domain ($S^{\alpha} \cap V^{cell}$). Therefore, we can determine the general location of cells in the tissue. We can conclude if a cell is surrounded only by other cells or it is in direct contact with the substrate.

Dynamic meshing: FE discretization

To generate a mesh for the finite element analysis (M^{FEM}), we create a Delaunay triangulation of a set of points ($DT(P)$) as shown in equation (6) and Figure 2C. In order to obtain a coherent mesh with

coincident nodes, the triangulation is constructed by points of the cell domain and the substrate domain. In the cellular domain, we use cell centroids (S^{cell}), Voronoi polygon vertices (V^{cell}) and points from the alpha shape curves (S^{α}). In the substrate domain, we create a regular grid of points (S^{grid}):

Equation (6)
$$U^{FEM} = S^{cell} \cup V^{cell} \cup S^{\alpha} \cup S^{grid}$$
$$M^{FEM} = DT\left(U^{FEM}\right)$$

The dynamic mesh generation is a key aspect of our approach since, in this process, we map the information from discrete cell model and all the geometrical traits to the continuum model. Here, we keep the relation between centroids and vertices and their corresponding nodes in the mesh. Therefore, we are also able to pass information from the continuum model to the discrete model.

2.4 Force generation

To model the cell mechanical behavior, we must consider the forces that generate each one individually and the forces generated by their interactions. First, we describe cell-cell interaction forces ($\boldsymbol{F}^{interaction}$) using a potential with a repulsive and an attractive term. Second, the contraction force ($\boldsymbol{F}^{contraction}$) that is generated in each cell by its cytoskeleton. Finally, two different collective migration modes that create forces in the tissue: cell crawling ($\boldsymbol{F}^{crawl}$) and purse-string ($\boldsymbol{F}^{purse-string}$) [3,31]. In summary, we define the forces that cells generate as follows:

Equation (7) $\boldsymbol{F}^{cell} = \boldsymbol{F}^{interaction} + \boldsymbol{F}^{contraction} + \boldsymbol{F}^{crawl} + \boldsymbol{F}^{purse-string}$ These cell forces ($\boldsymbol{F}^{cell}$) are the ones referenced before in the equation (2A), where it is described the force equilibrium in the cell material. In this section, we describe in detail each one of these forces and how we model them in our discrete approach.

Figure 3. Force generation. A) Cell-cell interaction force $F_{j,i}^{interaction}$ between cell S_i^{cell} and its neighboring cell $S_{j,i}^{neighbors}$. The distance between cells is denoted by $r_{j,i}$. B) Contraction force in the vertices ($V_{k,i}^{cell}$) of the cell S_i^{cell}. This force depends on the edges lengths $l_{k,i}^{R}$ and $l_{k,i}^{L}$ related to the vertex *k*. We apply the same force with inverted sign to the cell centroid. C) Cell crawling forces $F_{k,i}^{crawling}$ are similar to contraction forces, but they are only applied to vertices that are on the cell-substrate interface. D) In purse-string migration, we generate a ring around the gap in the monolayer that connects cell vertices *m* located on the cell-substrate interface. The contraction of the ring generates a force $F_{m,i}^{purse-string}$.

Cell-cell interaction

To model the direct interaction between cells, we use a potential that approximates several biophysical phenomena. In fact, we consider the average effect of cell adhesion, cytoskeleton interaction, and volume exclusion.

We use an interaction force between particles *i* and *j* ($F_{j,i}^{interaction}$) that is derived from Lennard-Jones potential as it is shown in equation (8). In this work, this potential depends on the distance between cells ($r_{j,i}$) and the sum of cell virtual radii ($r_m = R_i + R_j$). In addition, there is a parameter ε that modulates the magnitude of the interaction forces. This potential presents a repulsive and an attractive term and, therefore, a distance of equilibrium (r_m) where both effects compensate.

Equation (8) $$F_i^{interaction} = \sum_j F_{j,i}^{interaction}(r) = 12 \cdot \varepsilon \cdot \sum_j \left[\left(\frac{r_m^{12}}{r_{j,i}^{13}} \right) - \left(\frac{r_m^{6}}{r_{j,i}^{7}} \right) \right]$$

Unlike other forces in our modeling approach, cell-cell interaction forces depend exclusively on the discrete cell model. These forces are calculated considering all neighboring cells ($S_i^{neighbors}$), and the resultant force is located at the cell centroid position as shown in Figure 3A. For each pair of cells, the direction of the force is defined from the cell centroid to the neighbor cell centroid. Finally, the effect of the ε parameter in the monolayer is described in detail in a previous work [32].

Actomyosin contraction

To model the effect of actomyosin contraction in cell cytoskeleton, we assume a constant net force for the whole cell ($F_i^{contraction}$). However, we model locally these forces on each vertex *k* of the polygonal representation of the cell *i* ($V_{k,i}^{cell}$) as Figure 3B illustrates. We show in equation (9) that the magnitude of the force on each vertex ($F_{k,i}^{contraction}$) is a constant ($K^{contraction}$) multiplied by a length ratio associated to the vertex. This ratio is equal to the sum of half-lengths of both edges connected by the vertex ($l_{k,i}^{L}$ and $l_{k,i}^{R}$) divided by the total cell perimeter (P_i).

Equation (9) $$F_i^{contraction} = \sum_k F_{k,i}^{contraction} = K^{contraction} \cdot \sum_k \left(\frac{l_{k,i}^{L} + l_{k,i}^{R}}{2 \cdot P_i} \right)$$

These force vectors are directed from cell vertex to the cell centroid. In addition, we apply a similar force with the inverse sign on the cell centroid (S_i^{cell}).

The reasoning behind this force model is that cytoskeleton contraction driven by actomyosin is homogeneous in non-polarized cells [33]. Thus, we are assuming that in this particular contraction force there is no polarization beyond the apicobasal one.

Cell Crawling

Cell crawling is a migration mode in which cell extends a protrusion that adheres to the substrate and pulls from it [3,4,31]. We model this phenomenon like the actomyosin contraction but only considering cell vertices that are on the cell-substrate boundaries ($\Gamma^{cell-substrate}$) and its own constant (K^{crawl}), as shown in equation (10). Hence, these forces (F_i^{crawl}) are not present on the shared faces between cells inside the monolayer as illustrated in Figure 3C.

Equation (10) $F_i^{crawl} = \sum_k F_{k,i}^{crawl} = K^{crawl} \cdot \sum_k \left(\frac{l_{k,i}^L + l_{k,i}^R}{2 \cdot P_i} \right)$ *for* $V_{k,i}^{cell} \cap \Gamma^{cell-substrate}$

In fact, we are assuming here that there is a front-back polarization in the cells that is directed towards substrate domain. Therefore, only cells in direct contact with the interface cell-substrate domain are playing a leading role in the crawling migration mode.

Purse-string

Purse-string is a migration mode only present in multi-cellular systems with matured cell-cell adhesions [1,3]. This migration mode is found typically in gap closing and wound healing biological processes. In purse-string migration, cells create an actomyosin string that surrounds the gap in the layer. This inter-cellular string contracts and generates forces that, effectively, pull from cells to close the gap.

As Figure 3D shows, we model these forces ($F^{purse-string}$) creating a virtual string that connects cells located around a gap in the tissue. Then, we generate a contraction force on vertices $V_{m,i}^{cell}$ that are shared between cell *i* and its neighbors *j*, and also located on the cell-substrate interface ($\Gamma^{cell-substrate}$).:

Equation (11) $F_{j,i}^{purse-string} = K^{purse-string}$ *for* $V_{m,i}^{cell} = V_{k,i}^{cell} \cap V_j^{cell} \cap \Gamma^{cell-substrate}$

We assume that these forces are constant ($K^{purse-string}$) in our approach.

3 Numerical implementation

For the computational implementation of our approach, we use several open-source tools and libraries to extend our own code and to process the results of the simulations. We develop this simulation framework in C++ using functionality of the C++11 revision and, in addition, we create some Python tools for the representation and the analysis of the results. In fact, we rely on third-party libraries that are demonstrably efficient and well tested. The computational workflow is represented and described in detail in Figure 4.

Figure 4. Computational workflow. First, we initialize the system variables and, afterward, we enter the main loop of the calculation. In the agent-based model, we compute the life cycle and cell internal clock is updated. Further, we determine here which cells divide. We use the information of the agent-based model to generate the geometry and the forces in the system. Some forces also depend on the Voronoi diagram representation of the cells and the alpha shapes. Later, we generate the FE mesh and we apply the forces to mesh nodes that correspond to cell centroids and cell vertices. We solve the FE problem after we have defined the material properties of each monolayer domain. Last, we use the deformed mesh to update cells position in the next step.

In this work, the discrete cell model is developed completely from scratch including its life cycle model. Additionally, the force generation models are also programmed exclusively for this simulating approach using our own code.

We use *CGAL* library [34] to compute most of the geometrical algorithms explained before. This library is focused on providing tools for mathematical operations with complex geometries. We use *exact predicates and exact constructions kernel* to reduce numerical errors in the geometrical operations as much as possible. In addition to the core packages, we use several *CGAL* modules: *2D Triangulation*, *2D Polygons*, *2D Voronoi Diagram Adaptor*, *2D Alpha Shapes* and *Bounding Volumes*.

Moreover, we use *deal.II* library to solve the mechanical problem by the FEM [35]. This library is a very powerful and flexible tool that provides base classes for the basic components to develop a FEM application. In addition, it also provides useful interfaces with external solvers, for instance, *UMFPack* [36] that is the one we use. Additionally, we create a refinement method to convert the triangular mesh into a quadrilateral mesh since *deal.II* does not support triangles. We subdivide each triangle into three quadrilaterals as shown in detail in Figure S2. We create an intermediate translation layer between geometrical representation and *deal.II* to manage the mesh and the information associated with it.

Finally, we develop a legacy *VTK* parser to represent results from the discrete model and *CGAL* structures. In addition, we visualize these files and generate animations using *Paraview* [37]. We use

seaborn [38], *pandas* [39] and an in-house python library to perform statistics on the simulation raw data. Moreover, we also rely on *seaborn* to plot the results of the statistical analysis.

4 Numerical examples

To validate our approach, we present here two examples of application that are found in the literature to describe epithelial tissue mechanics. First, we simulate a cell monolayer over a substrate that presents a stiffness gradient [4,40]. In this biological scenario, we study cell collective migration to stiffer environments, this phenomenon is also known as durotaxis. Second, we analyze how mechanical interactions between cells and substrate affect gap closing process in epithelial monolayers [1,27].

For each case shown in the following results, we have run at least N=5 simulations in order to calculate the statistics. In addition, simulation parameters are defined in the tables shown for each example (Table 1 and Table 2), and we do not change these default values unless it is explicitly indicated.

4.1 Collective durotaxis

Durotaxis is the biological process in which cells sense and follow gradients on the extracellular matrix [4]. Cell crawling is the migration mode that predominates in the case of collective durotaxis. Therefore, cells located at the edges of the layer extend protrusions that adhere to the substrate. Afterward, the contraction of this protrusion produces a deformation of the cell and the substrate. This deformation depends on the rigidity of extracellular matrix and defines the net displacement of the cell center of mass. When substrates present non-uniform stiffness, the substrate deformations are larger on the zones with lower stiffness, and, therefore, cell center of mass movement is reduced for the same contraction force. On the contrary, cells are effectively displaced larger distances on the stiffer zones since substrate deformations are smaller. Consequently, a cell monolayer will effectively migrate over a substrate that presents a stiffness gradient.

Moreover, it has been observed experimentally that force transmission to the substrate in collective cell migration is mostly concentrated at the monolayer edges [4]. Thus, we assume that interaction between cell monolayer and substrate can be modeled applying forces only on the interface that separates both domains as it is shown in Figure S3. To simulate this process using our modeling approach, we consider forces that are generated by cell-cell interactions, cell contraction and cell crawling models explained in the previous sections. In this case, we do not use purse-string forces since it is not relevant for this phenomenon. Purse-string migration mechanism is mainly found in gap closure or wound healing processes, and not in the case of monolayer expansion shown in this example [1,3].

Finally, we simulate three different scenarios to study collective durotaxis changing substrate properties: uniform stiffness, steep stiffness gradient, and shallow stiffness gradient. For two later cases, we use a linear stiffness gradient where the side with lower stiffness is always on the left of the simulated substrate and the stiffer side is on the right. The difference between steep and shallow gradient is just the slope of the linear function that defines the stiffness of the substrate.

Results and Discussion

Table 1. Collective durotaxis parameters.

General parameters	
Cell radius *(μm)* – R_i	10
Cell layer size *(μm)*	500x1000
Substrate size *(μm)*	2500x1000
Alpha shapes parameter – α	150
Proliferation parameters	
Growth rate – λ^{cycle}	0,05*
Proliferation threshold – θ^{cycle}	100*
Cell domain mechanical properties	
Cell domain stiffness – E^{cell} ($\mu N/\mu m^2$)	0,02 [5]
Cell domain Poisson's ratio – $\nu^{\Omega cell}$	0,49** [5]
Substrate domain mechanical properties	
Substrate domain stiffness – $E^{substrate}$ ($\mu N/\mu m^2$)	0,02 [4,5]
Substrate domain Poisson's ratio – $\nu^{\Omega substrate}$	0,49** [5]
Uniform stiffness slope – *m (kPa/mm)*	0
Shallow stiffness gradient slope – *m (kPa/mm)*	15 [4]
Step stiffness gradient slope – *m (kPa/mm)*	57 [4]
Force generation parameters	
Cell-cell interaction parameter – ε (μN)	1,00E-04 [32]
Cell contraction constant – $K^{contraction}$ (μN)	5,00E-04 [4, 33]
Cell crawling constant – K^{crawl} (μN)	1,50E-03
Purse-string constant – $K^{purse\text{-}string}$ (μN)	0

* Approximately 2% of cells proliferating

** Approximately incompressible

We calculate the angular distribution of cell trajectories on the three substrates to understand how substrate stiffness gradients affect cell migration. This distribution is obtained using the angle between cell velocity vector direction and X axis. Instantaneous cell velocity vector is computed from the cell trajectories for every 50 simulation steps. This metric lets us understand if cells show a preferential direction during migration. In Figure 5A, we observe that cells present durotaxis only when a stiffness gradient is present (see Video S4 and Video S6), as it was described in previous experimental studies[4]. In addition, the cell motion persistence is intensified by using steeper stiffness gradients. Therefore, cell migration over substrates with a steep stiffness gradient is more polarized than over substrates with a shallow stiffness gradient.

Figure 5. (A) Angular distribution of cell trajectory for the three different substrates. Cells only show a preferential direction to migrate when a stiffness gradient is present. (B) Displacements of monolayer center of mass depending on the initial substrate stiffness. Collective durotaxis is reduced on stiffer substrates.

Furthermore, we analyze the displacement of the monolayer center of mass over substrates with different average stiffness. These results let us determine how durotaxis phenomenon is affected by extracellular matrix rigidity. Hence, we calculate the displacement of center of mass using the average distance from left border to right border of the monolayer. We predict that durotaxis is reduced when substrate global stiffness increases as shown in Figure 5B. On the other hand, on lower stiffness substrates within the stiffness range analyzed, the durotaxis is more pronounced when the gradient is stronger.

On Figure 6A,B, we can observe how cell displacements are distributed during the simulation. In the case with a substrate stiffness gradient, cells are moving to the stiffer side of the substrate and the displacements are higher in gradient direction. In the uniform stiffness case, cell displacements are distributed without a preferential direction. Finally, stresses in the monolayer accumulate on the interface between the substrate and the monolayer in both cases as seen in Figure 6C,D (see Video S5 and Video S7).

Figure 6. (A, B) Total distance traveled by cells. The initial shape of the monolayer is shown in red. We observe that when stiffness gradient is present cells show a preferential direction to migrate. (C, D) Principal stresses in the material. We observe that in both uniform and gradient substrates stresses are accumulated in the monolayer/substrate interface.

These simulation results are compatible with the experimental data from *Sunyer et al. [4]*. Moreover, they validate several of our model considerations about collective cell migration and cell interaction with the substrate. In particular, the assumption that force transmission between cell monolayer and substrate occurs exclusively in the monolayer borders. We predict that durotaxis effectiveness decreases when the average stiffness of the substrate increases, that is also one of the main conclusions of *Sunyer et al. [4]* work.

The underlying migration mechanism relies on the fact that the stiffer side of the substrates are deformed less than the side of the lower stiffness by the same cell contraction force. In consequence, cells that pull from stiffer side of the substrate move in a more efficient way. At the collective level, cells that pull from the lower stiffness side of the monolayer-substrate interface produce larger substrate deformations and, therefore, lower cell displacements. Otherwise, cells in the edge of the monolayer in contact with the stiffer side move larger distances exerting the same contraction force. This phenomenon produces an effective displacement of the monolayer to the stiffer side of the substrate and the observed collective durotaxis.

Furthermore, cell proliferation is also present in *Sunyer et al.* experiments of collective durotaxis in expanding epithelial layers. Hence, we include cell life cycle in order to simulate these experiments under similar conditions. We adjust our life cycle parameters to obtain an approximated 2-3% of cells proliferating at the same time. Although this ratio is not explicitly present in the *Sunyer et al. [4]* study, we choose that range considering the measured values in proliferating epithelial tissues from other studies [41,42]. In any case, *Sunyer et al.* demonstrated that proliferation is not dependent on substrate stiffness and, therefore, collective durotaxis is mainly driven by the mechanical equilibrium balance.

Finally, it is also demonstrated here that using a transient vertex model combined with a continuum material model is a reliable option to simulate complex mechanical phenomena in cell monolayers.

4.2 Gap closure

Table 2. Gap closure parameters.

General parameters	
Cell radius *(μm)* – R_i	10
Cell layer size *(μm)*	1000x1000
Substrate size *(μm)*	1000x1000
Gap size *(μm)*	180x180
Alpha shapes parameter – α	150
Proliferation parameters	
Growth rate – λ^{cycle}	0*
Proliferation threshold – θ^{cycle}	0*
Cell domain mechanical properties	
Cell domain stiffness – E^{cell} ($\mu N/\mu m^2$)	0,02 [5]
Cell domain Poisson's ratio – $\nu^{\Omega cell}$	0,49** [5]
Substrate domain mechanical properties	
Substrate domain stiffness – $E^{substrate}$ ($\mu N/\mu m^2$)	0,02 [5]
Substrate domain Poisson's ratio – $\nu^{\Omega substrate}$	0,49** [5]
Force generation parameters	
Cell-cell interaction parameter – ε (μN)	1,00E-4 [32]
Cell contraction constant – $K^{contraction}$ (μN)	5,00E-4 [4, 33]
Cell crawling constant – K^{crawl} (μN)	5,00E-04
Purse-string constant – $K^{purse\text{-}string}$ (μN)	1,50E-03

* No proliferation

** Approximately incompressible

In contrast to monolayer expansion, epithelial cells can present several migration modes during gap closing. It has been observed that depending on gap size, tissue type and environmental conditions the way to close a gap in the tissue may change, however, cell crawling and purse-string contraction are the most common migration modes [1,3,27,30]. Moreover, these modes can even be present at the same time and compete between them to dominate the closing process.

Here, we aim to analyze how these migration modes affect a gap closing process using our modeling approach. We generate a confluent monolayer and then remove some cells from the center to create a gap. In this case, we consider all the forces explained before: cell-cell interaction, contraction, cell crawling and purse-string. We focus our efforts on studying the effect of cell crawling and purse-string forces in this phenomenon.

Results and Discussion

To understand the effect of cell forces in gap closing, we quantify the area of the tissue gap using the alpha shapes and the cell average velocity. We compare how cells close the gap using purse-string and

crawling migration mode in Figure 7A,B. In fact, we observe different cell velocity profiles between migration modes. Purse-string migration presents a high initial velocity that decays rapidly. In contrast, cell crawling migration shows an almost constant velocity profile. Moreover, we observe a reduction of the curvature and a smoothing of the gap morphology in the case of purse-string migration as shown in Figure 7E (see Video S8). However, this curvature reduction is not observed in crawling migration mode. These results are in agreement with the experimental results found in [27].

Figure 7. (A, C, F) Average cell velocity during the simulation under different conditions. (B, D, G) Gap area during the simulation under different conditions. (A, B) Comparison between purse-string and crawling migration mode. (C, D) Parametric analysis of purse-string forces. (F, G) Parametric analysis of crawling forces. (E) Gap morphology with purse-string migration mode (top) and crawling migration mode (bottom).

In Figure 7C,D, we show a parametric analysis of the purse-string force effect in gap closing (see Video S9). The cell velocity presents a high initial value for all the cases followed by a notable velocity drop. In addition, gap area evolution during the simulation is highly non-linear. Moreover, we observe that gap closes faster for higher purse-string forces. However, cells never fill the gap when purse-string forces are too low ($0.5x10^{-3}\mu N$).

Furthermore, we show a parametric analysis of cell crawling forces in Figure 7F,G (see Video S10). We predict that for all cases gap closes faster when we increase crawling force. In contrast to purse-string, cells fill the gap even when we are using very low crawling forces and gap area profile is almost linear.

It has been previously reported that larger gaps are dominated mostly by cell crawling [1,3,27,30]. If we observe the results from our simulations, purse-string mechanism creates a very fast migration that decays quickly. Hence, our results are compatible with these observations since closing a large gap in a monolayer needs a constant migration force to complete the process. The initial peak of cell velocity during purse-string migration may facilitate the closure when the gap is small. In addition, the reduction of curvature and the gap border smoothing could also be beneficial in combination with cell crawling. In fact, exclusive cell crawling migration does not produce a homogeneous closure as it is shown in the work of *Ravasio et al.* [27] and *Brugués et al. [1]*. Therefore, purse-string may not be the main driving force in some gap closure cases, but it can help to smooth and homogenize the process.

In conclusion, we successfully reproduce here another collective migration phenomenon from a mechanical perspective. In our approach, we can study the effect of the two migration mechanisms separately. Moreover, we observe their effects at monolayer scale and we can still track the individual cell velocities and trajectories (see Video S8-S10).

5 Conclusions

We present here a novel approach to model collective migration in epithelial cell monolayers. In fact, we combine a discrete agent-based model that let us keep individual cell information with a continuum material model that can simulate tissue and substrate mechanical behavior. In this modeling approach, we also aim to build a framework from modular models. This design facilitates the inclusion of independent force models and decoupling some biophysical phenomena.

We demonstrate that our modeling approach is able to reproduce a variety of experimental results for durotaxis and gap closure processes. First, we analyze the assumption that force transmission between cell layer and substrate occurs right on the interface. This is valid for cases where monolayer is expanding, and, therefore, it is also applicable to durotaxis phenomenon. Further, our results predict the behavior of collective cell migration on substrate stiffness gradients [4]. Second, we reproduce and compare the effect of the principal migration mechanisms in gap closing process: cell crawling and purse-string contraction. We observe a very different response and gap morphology for the two migration modes. In fact, these results are compatible with the experimental results obtained by other authors that have extensively analyzed gap closure [1,3,27,30].

Unlike the classic vertex-based model, we can not control the shape of the cells explicitly since its generation is given by the cell centroids positions on the Voronoi diagram. Despite this can be considered a drawback of our approach, cell morphology is an emergent property of the system that depends on the cell spatial distribution. In fact, we are not really interested in controlling individual cell morphology, but in using the cell shape to more accurately distribute the forces generated in the layer.

In this work, we have assumed that stress dissipation in the monolayer due to cytoskeleton and cell-cell junctions restructuring is several orders of magnitude faster than cell rearrangements and migration on the layer [5,6,8,43]. Thus, we do not accumulate stresses in the monolayer material from one step to the next under this assumption. In fact, cells do not store its stress state either. Effectively, tissue evolution is time-dependent and presents a global viscoelastic behavior. Although we would need to accumulate these stresses to simulate very fast mechanical changes in the epithelial layer, this simplification is still valid for ‘slow’ migration and rearrangement processes shown here as examples of application. On the other hand, cell intercalation occurs spontaneously due to Voronoi tessellation. Therefore, the tissue stress due to rearrangements is directly related to forces generated by cells in their new location, in particular, cell-cell interaction and actomyosin contraction forces. In any case, we could accumulate stress in the material and model a non-instantaneous stress dissipation during the simulation, but it is out of the scope of this paper.

We believe that this modeling approach here presented offers a great flexibility and new possibilities to simulate cell layer mechanics which were not considered before. The combination of particle, transient vertex representation and continuum model may open new strategies to model other inherently 2D biological processes where cell and tissue mechanics are fundamental. For instance, it would be

possible to apply this approach to simulate processes where cells are driven by patterns on the substrate, cell transition between solid-like to fluid-like behavior or collisions between migrating cell monolayers.

6 Acknowledgments

This research was supported by the European Research Council (ERC) through project (ERC-2012-StG 306571) and the Spanish Ministry of Economy and Competitiveness (DPI2015-64221-C2-1-R).

We wish to thank all open-source projects that we have used for developing our work: *deal.II*, *CGAL*, *suitesparse*, *seaborn*, *matplotlib* and *Paraview*.

7 Supplementary Material

Figure S1. Cell division using the minimum ellipse. We model an oriented cell division over its shortest axis. To simulate this division, we generate an ellipse that is circumscribed in the cell polygonal representation. Since the polygonal representation of the cells is generated using the Voronoi diagram, we locate parent (S_i^{cell}) and daughter (S_j^{cell}) centroids on the ellipse major axis separated by a distance *d*. Therefore, the cell will be effectively divided by the shortest ellipse axis.

Figure S2. Mesh refinement. Our original FE mesh generated from the Delaunay triangulation is, by definition, composed by triangles. However, we use *deal.II* library to solve FE problem and, unfortunately, it does not support triangles. Hence, we must convert triangular elements to quadrilaterals. To overcome this issue, we refine each triangular element E of the mesh into three quadrilaterals E'_A, E'_B and E'_C. The vertices of these quadrilaterals are defined by the vertices of the triangle E, the midpoints of E edges (M_A, M_B and M_C) and the center of mass of E (C_E).

Figure S3. Force transmission between the monolayer and the substrate. The force transmission between expanding cell monolayer and substrate is mainly concentrated at the limits of the monolayer. Basically, forces are transmitted through the cell monolayer by the cell-cell junctions and to the substrate by cell-substrate adhesions. These cell-substrate adhesions are notably stronger at the monolayer limits. Therefore, we do not model the substrate under the cell monolayer since its role in the force transmission is negligible during collective migration.

Video S4. Cell displacements in a uniform substrate.

Video S5. Monolayer stresses in a uniform substrate.

Video S6. Cell displacements in a substrate with a stiffness gradient.

Video S7. Monolayer stresses in a substrate with a stiffness gradient.

Video S8. Comparison between purse-string and cell crawling forces.

Video S9. Parametric analysis of purse-string force.

Video S10. Parametric analysis of cell crawling force.

8 References

[1] A. Brugués, E. Anon, V. Conte, J.H. Veldhuis, M. Gupta, J. Colombelli, J.J. Muñoz, G.W. Brodland, B. Ladoux, X. Trepat, Forces driving epithelial wound healing, Nat. Phys. 10 (2014) 683–690. doi:10.1038/nphys3040.

[2] S.R.K. Vedula, G. Peyret, I. Cheddadi, T. Chen, A. Brugués, H. Hirata, H. Lopez-Menendez, Y. Toyama, L. Neves de Almeida, X. Trepat, C.T. Lim, B. Ladoux, Mechanics of epithelial closure over non-adherent environments, Nat. Commun. 6 (2015) 6111. doi:10.1038/ncomms7111.

[3] S. Begnaud, T. Chen, D. Delacour, R.-M. Mège, B. Ladoux, Mechanics of epithelial tissues during gap closure, Curr. Opin. Cell Biol. 42 (2016) 52–62. doi:10.1016/j.ceb.2016.04.006.

[4] R. Sunyer, V. Conte, J. Escribano, A. Elosegui-Artola, A. Labernadie, L. Valon, D. Navajas, J.M. Garcia-Aznar, J.J. Munoz, P. Roca-Cusachs, X. Trepat, Collective cell durotaxis emerges from long-range intercellular force transmission, Science (80-.). 353 (2016) 1157–1161. doi:10.1126/science.aaf7119.

[5] A.R. Harris, L. Peter, J. Bellis, B. Baum, A.J. Kabla, G.T. Charras, Characterizing the mechanics of cultured cell monolayers, Proc. Natl. Acad. Sci. 109 (2012) 16449–16454. doi:10.1073/pnas.1213301109.

[6] T.P.J. Wyatt, A.R. Harris, M. Lam, Q. Cheng, J. Bellis, A. Dimitracopoulos, A.J. Kabla, G.T. Charras, B. Baum, Emergence of homeostatic epithelial packing and stress dissipation through divisions oriented along the long cell axis, Proc. Natl. Acad. Sci. 112 (2015) 5726–5731. doi:10.1073/pnas.1420585112.

[7] A.R. Harris, A. Daeden, G.T. Charras, Formation of adherens junctions leads to the emergence of a tissue-level tension in epithelial monolayers, J. Cell Sci. 127 (2014) 2507–2517. doi:10.1242/jcs.142349.

[8] C. Guillot, T. Lecuit, Mechanics of Epithelial Tissue Homeostasis and Morphogenesis, Science (80-.). 340 (2013) 1185–1189. doi:10.1126/science.1235249.

[9] P. Van Liedekerke, M.M. Palm, N. Jagiella, D. Drasdo, Simulating tissue mechanics with agent-based models: concepts, perspectives and some novel results, Comput. Part. Mech. 2 (2015) 401–444. doi:10.1007/s40571-015-0082-3.

[10] B.A. Camley, W.-J. Rappel, Physical models of collective cell motility: from cell to tissue, J. Phys. D. Appl. Phys. 50 (2017) 113002. doi:10.1088/1361-6463/aa56fe.

[11] E.A. Novikova, M. Raab, D.E. Discher, C. Storm, Persistence-Driven Durotaxis: Generic, Directed Motility in Rigidity Gradients, Phys. Rev. Lett. 118 (2017) 78103. doi:10.1103/PhysRevLett.118.078103.

[12] N. Sepúlveda, L. Petitjean, O. Cochet, E. Grasland-Mongrain, P. Silberzan, V. Hakim, Collective Cell Motion in an Epithelial Sheet Can Be Quantitatively Described by a Stochastic Interacting Particle Model, PLoS Comput. Biol. 9 (2013) e1002944. doi:10.1371/journal.pcbi.1002944.

[13] B. Smeets, R. Alert, J. Pešek, I. Pagonabarraga, H. Ramon, R. Vincent, Emergent structures and dynamics of cell colonies by contact inhibition of locomotion, Proc. Natl. Acad. Sci. 113 (2016) 14621–14626. doi:10.1073/pnas.1521151113.

[14] D. Bi, J.H. Lopez, J.M. Schwarz, M.L. Manning, A density-independent rigidity transition in biological tissues, Nat. Phys. 11 (2015) 1074–1079. doi:10.1038/nphys3471.

[15] A.J. Loza, S. Koride, G. V. Schimizzi, B. Li, S.X. Sun, G.D. Longmore, Cell density and actomyosin contractility control the organization of migrating collectives within an epithelium, Mol. Biol. Cell. 27 (2016) 3459–3470. doi:10.1091/mbc.E16-05-0329.

[16] J.-A. Park, J.H. Kim, D. Bi, J.A. Mitchel, N.T. Qazvini, K. Tantisira, C.Y. Park, M. McGill, S.-H. Kim, B. Gweon, J. Notbohm, R. Steward Jr, S. Burger, S.H. Randell, A.T. Kho, D.T. Tambe, C. Hardin, S.A. Shore, E. Israel, D.A. Weitz, D.J. Tschumperlin, E.P. Henske, S.T. Weiss, M.L. Manning, J.P. Butler, J.M. Drazen, J.J. Fredberg, Unjamming and cell shape in the asthmatic airway epithelium, Nat. Mater. 14 (2015) 1040–1048. doi:10.1038/nmat4357.

[17] D. Bi, X. Yang, M.C. Marchetti, M.L. Manning, Motility-driven glass and jamming transitions in biological tissues, Phys. Rev. X. 6 (2016) 1–12. doi:10.1103/PhysRevX.6.021011.

[18] D.L. Barton, S. Henkes, C.J. Weijer, R. Sknepnek, Active Vertex Model for cell-resolution description of epithelial tissue mechanics, PLOS Comput. Biol. 13 (2017) e1005569. doi:10.1371/journal.pcbi.1005569.

[19] P. Mosaffa, A. Rodríguez-Ferran, J.J. Muñoz, Hybrid cell-centred/vertex model for multicellular systems with equilibrium-preserving remodelling, (2017) 1–33. doi:10.1002/cnm.2928.

[20] T. Odenthal, B. Smeets, P. Van Liedekerke, E. Tijskens, H. Van Oosterwyck, H. Ramon, Analysis of Initial Cell Spreading Using Mechanistic Contact Formulations for a Deformable Cell Model, PLoS Comput. Biol. 9 (2013) e1003267. doi:10.1371/journal.pcbi.1003267.

[21] A. Moure, H. Gomez, Phase-field model of cellular migration: Three-dimensional simulations in fibrous networks, Comput. Methods Appl. Mech. Eng. 320 (2017) 162–197. doi:10.1016/j.cma.2017.03.025.

[22] A. Czirók, K. Varga, E. Méhes, A. Szabó, Collective cell streams in epithelial monolayers depend on cell adhesion, New J. Phys. 15 (2013) 75006. doi:10.1088/1367-2630/15/7/075006.

[23] M.M. Palm, R.M.H. Merks, Vascular networks due to dynamically arrested crystalline ordering of elongated cells, Phys. Rev. E - Stat. Nonlinear, Soft Matter Phys. 87 (2013). doi:10.1103/PhysRevE.87.012725.

[24] J. Escribano, M.T. Sánchez, J.M. García-Aznar, A discrete approach for modeling cell–matrix adhesions, Comput. Part. Mech. 1 (2014) 117–130. doi:10.1007/s40571-014-0006-7.

[25] T. Heck, B. Smeets, S. Vanmaercke, P. Bhattacharya, T. Odenthal, H. Ramon, H. Van Oosterwyck, P. Van Liedekerke, Modeling extracellular matrix viscoelasticity using smoothed particle hydrodynamics with improved boundary treatment, Comput. Methods Appl. Mech. Eng. 322 (2017) 515–540. doi:10.1016/j.cma.2017.04.031.

[26] J.C. Arciero, Q. Mi, M.F. Branca, D.J. Hackam, D. Swigon, Continuum Model of Collective Cell Migration in Wound Healing and Colony Expansion, Biophys. J. 100 (2011) 535–543. doi:10.1016/j.bpj.2010.11.083.

[27] A. Ravasio, I. Cheddadi, T. Chen, T. Pereira, H.T. Ong, C. Bertocchi, A. Brugues, A. Jacinto, A.J. Kabla, Y. Toyama, X. Trepat, N. Gov, L. Neves de Almeida, B. Ladoux, Gap geometry dictates epithelial closure efficiency, Nat. Commun. 6 (2015) 7683. doi:10.1038/ncomms8683.

[28] C. Valero, E. Javierre, J.M. García-Aznar, M.J. Gómez-Benito, Nonlinear finite element simulations of injuries with free boundaries: Application to surgical wounds, Int. J. Numer. Method. Biomed. Eng. 30 (2014) 616–633. doi:10.1002/cnm.2621.

[29] P. Moreo, J.M. García-Aznar, M. Doblaré, Modeling mechanosensing and its effect on the migration and proliferation of adherent cells, Acta Biomater. 4 (2008) 613–621. doi:10.1016/j.actbio.2007.10.014.

[30] E. Anon, X. Serra-Picamal, P. Hersen, N.C. Gauthier, M.P. Sheetz, X. Trepat, B. Ladoux, Cell crawling mediates collective cell migration to close undamaged epithelial gaps, Proc. Natl. Acad. Sci. 109 (2012) 10891–10896. doi:10.1073/pnas.1117814109.

[31] X. Trepat, M.R. Wasserman, T.E. Angelini, E. Millet, D.A. Weitz, J.P. Butler, J.J. Fredberg, Physical forces during collective cell migration, Nat. Phys. 5 (2009) 426–430. doi:10.1038/nphys1269.

[32] I. González-Valverde, J.M. García-Aznar, A hybrid computational model to explore the topological characteristics of epithelial tissues, Int. J. Numer. Method. Biomed. Eng. 33 (2017) e2877. doi:10.1002/cnm.2877.

[33] S.X. Sun, S. Walcott, C.W. Wolgemuth, Cytoskeletal cross-linking and bundling in motor-independent contraction, Curr. Biol. 20 (2010) R649–R654. doi:10.1016/j.cub.2010.07.004.

[34] The CGAL Project, CGAL User and Reference Manual, CGAL Editor. Board. (2017).

[35] D. Arndt, W. Bangerth, D. Davydov, T. Heister, L. Heltai, M. Kronbichler, M. Maier, J.-P. Pelteret, B. Turcksin, D. Wells, The deal.II Library, Version 8.5, J. Numer. Math. (2017). doi:10.1515/jnma-2017-0058.

[36] T.A. Davis, Algorithm 832, ACM Trans. Math. Softw. 30 (2004) 196–199. doi:10.1145/992200.992206.

[37] U. Ayachit, The ParaView Guide: A Parallel Visualization Application, Kitware, 2015.

[38] M. Waskom, O. Botvinnik, P.H. Lee, Y. Halchenko, S. Lukauskas, J.B. Cole, J. Warmenhoven, J. de Ruiter, S. Hoyer, J. Vanderplas, S. Villalba, G. Kunter, E. Quintero, M. Martin, A. Miles, K. Meyer, T. Augspurger, T. Yarkon, seaborn, (2016). doi:10.5281/zenodo.54844.

[39] W. McKinney, Data Structures for Statistical Computing in Python, in: S. van der Walt, J. Millman (Eds.), Proc. 9th Python Sci. Conf., 2010: pp. 51–56.

[40] C.M. Lo, H.B. Wang, M. Dembo, Y.L. Wang, Cell movement is guided by the rigidity of the substrate, Biophys. J. 79 (2000) 144–152. doi:10.1016/S0006-3495(00)76279-5.

[41] T. Aegerter-Wilmsen, A.C. Smith, A.J. Christen, C.M. Aegerter, E. Hafen, K. Basler, Exploring the effects of mechanical feedback on epithelial topology, Development. 137 (2010) 499–506. doi:10.1242/dev.041731.

[42] S.A. Gudipaty, J. Lindblom, P.D. Loftus, M.J. Redd, K. Edes, C.F. Davey, V. Krishnegowda, J. Rosenblatt, Mechanical stretch triggers rapid epithelial cell division through Piezo1, Nature. 543 (2017) 118–121. doi:10.1038/nature21407.

[43] T. Wyatt, B. Baum, G. Charras, A question of time: tissue adaptation to mechanical forces, Curr. Opin. Cell Biol. 38 (2016) 68–73. doi:10.1016/j.ceb.2016.02.012.

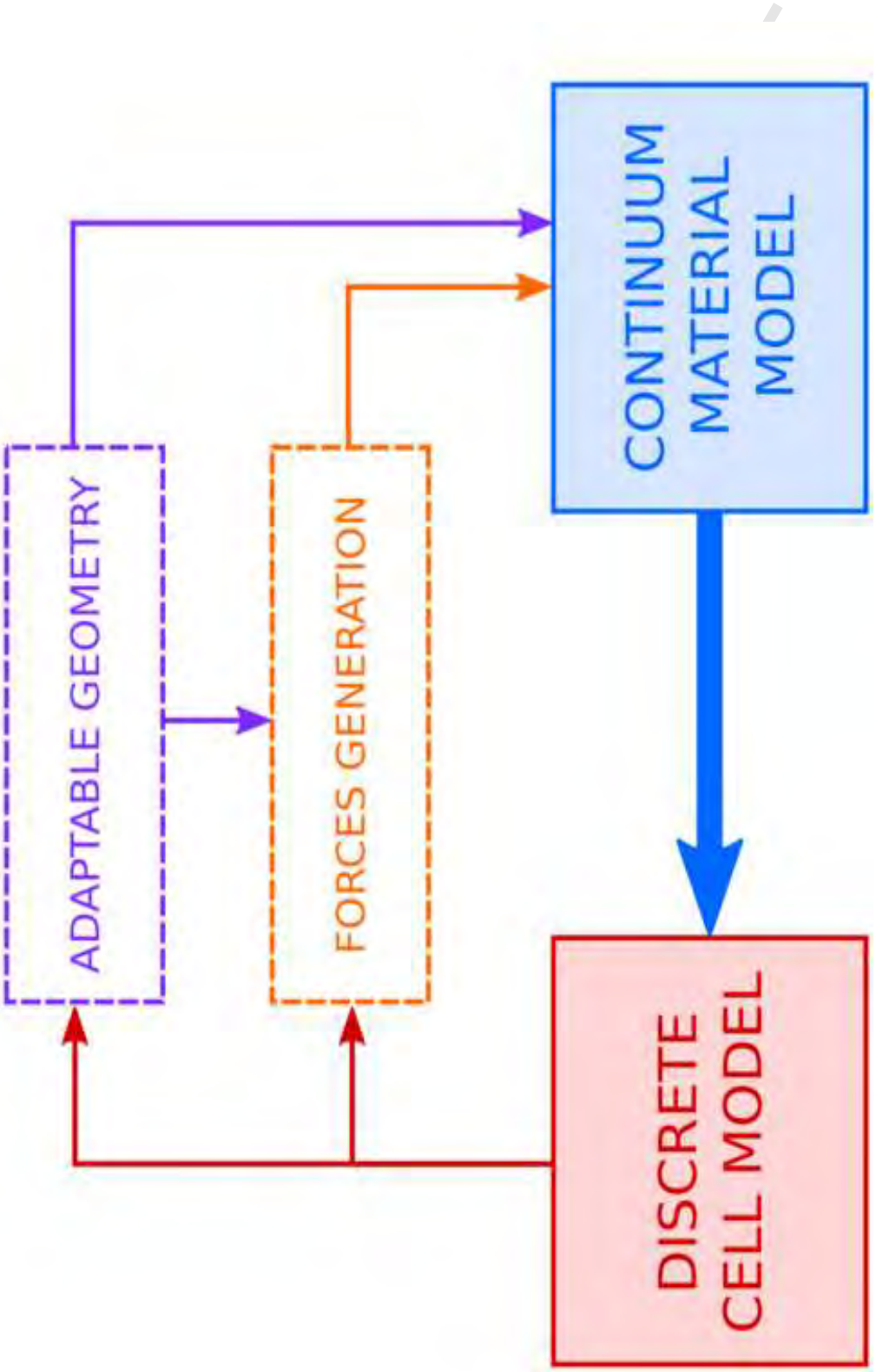

Figure
Click here to download high resolution image

Figure
Click here to download high resolution image

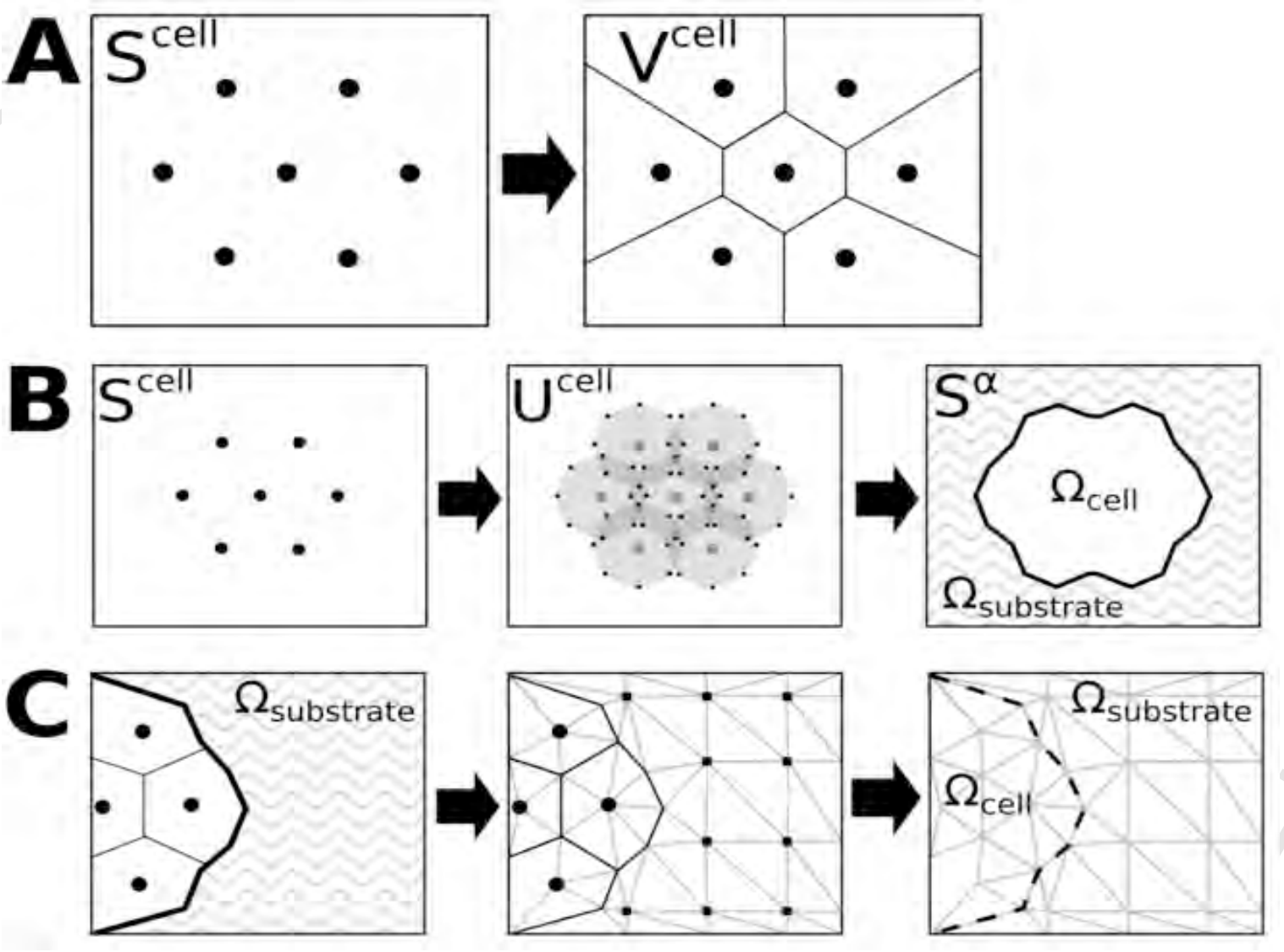

Figure
Click here to download high resolution image

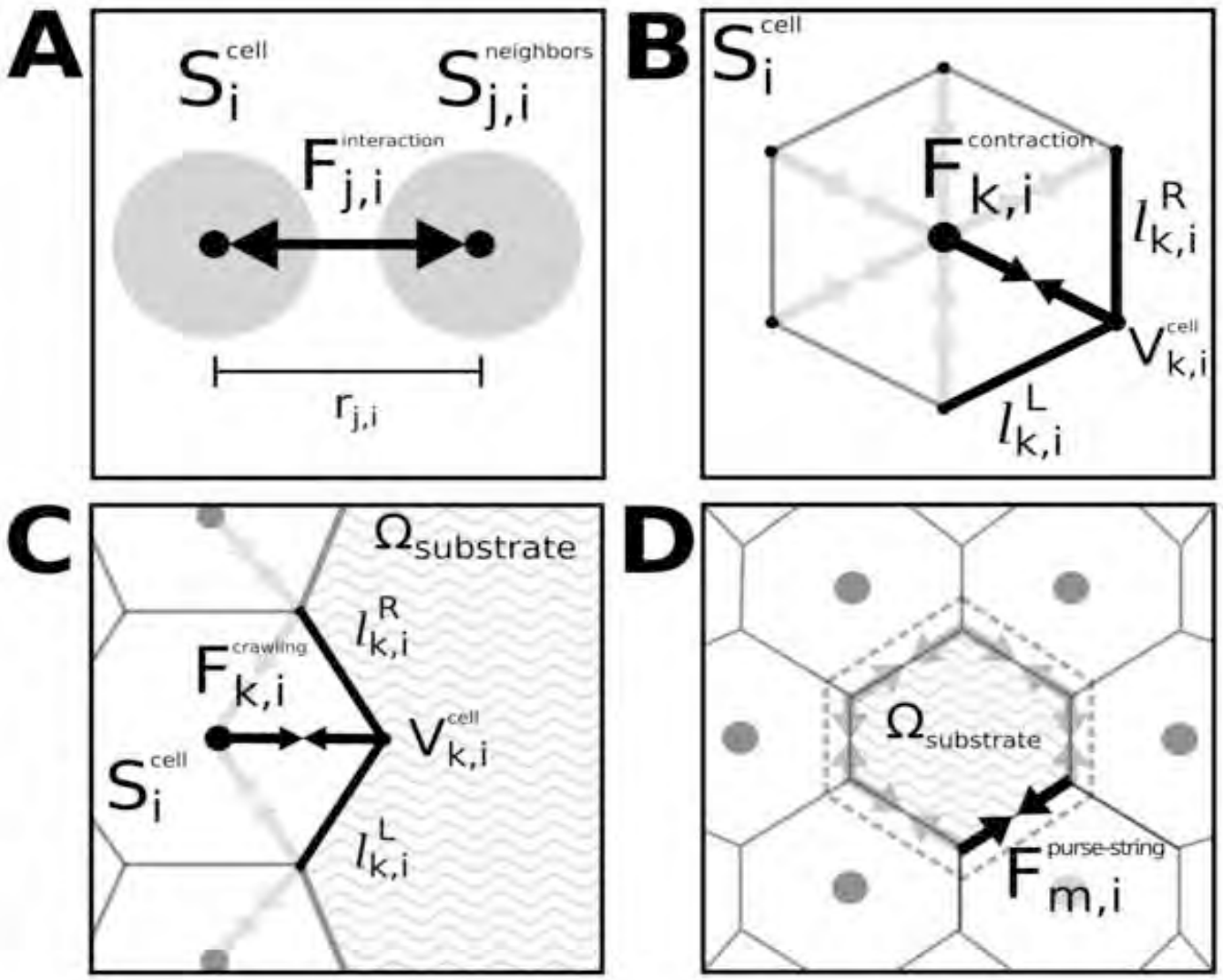

Figure
Click here to download high resolution image

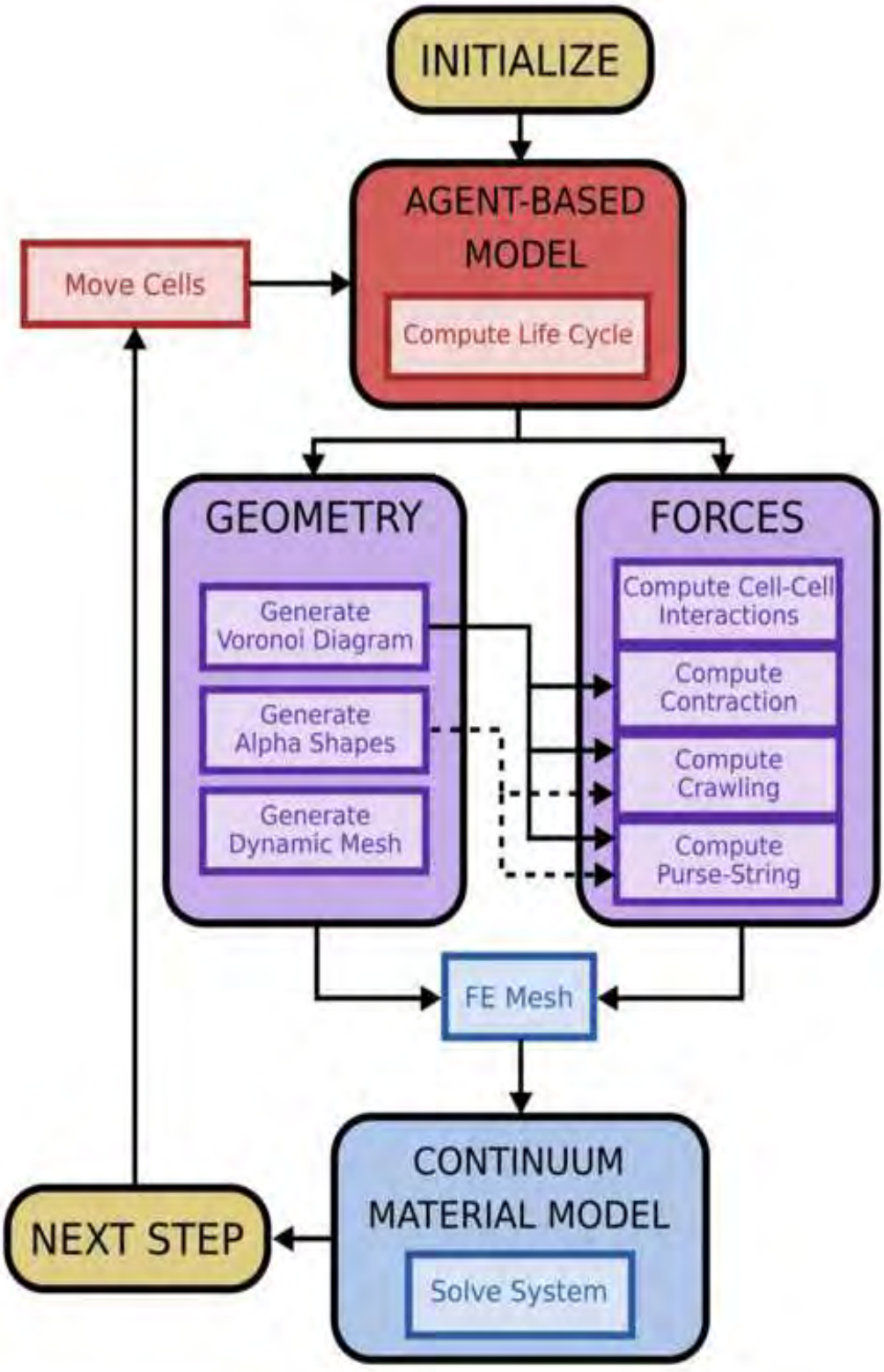

Figure
Click here to download high resolution image

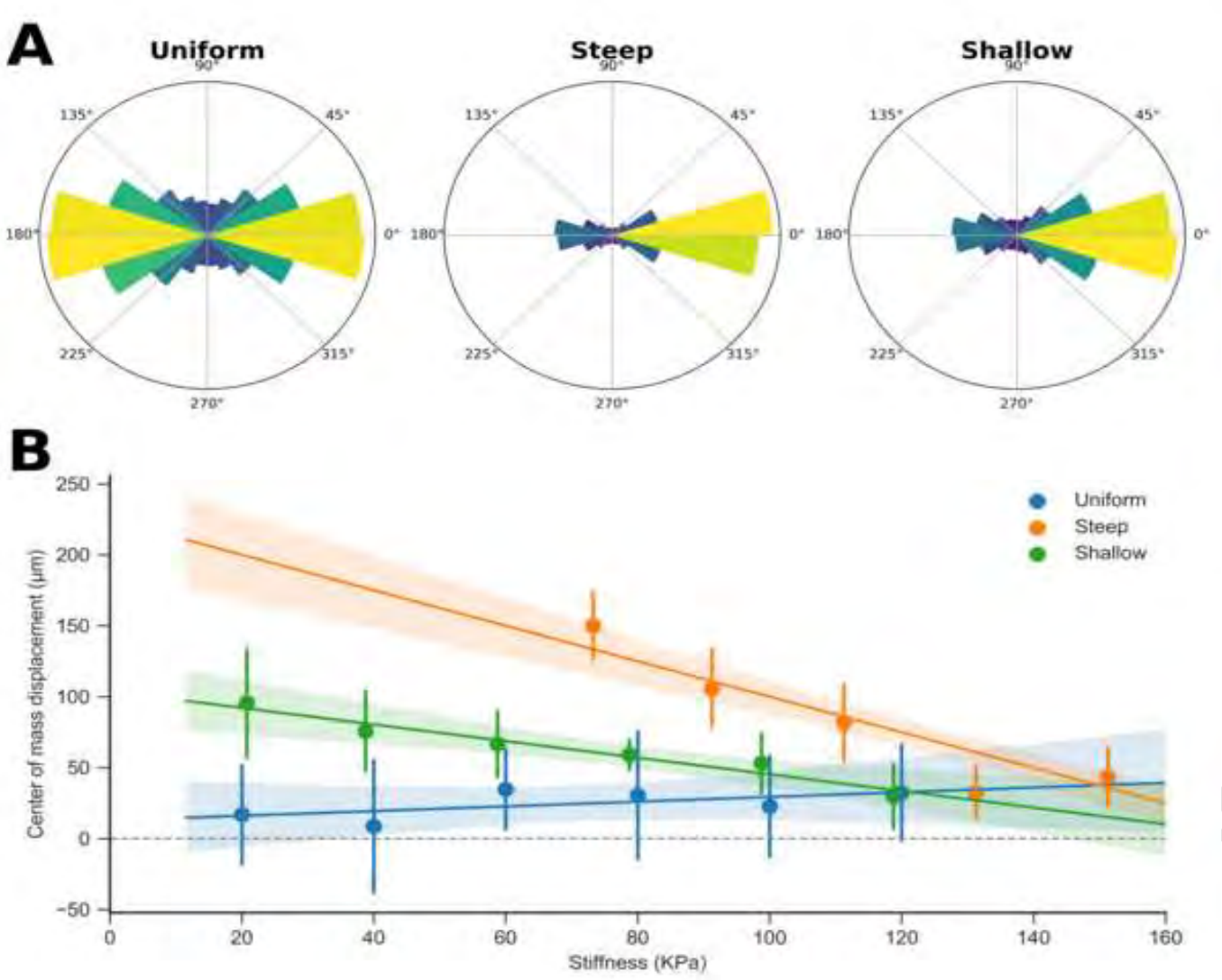

Figure
Click here to download high resolution image

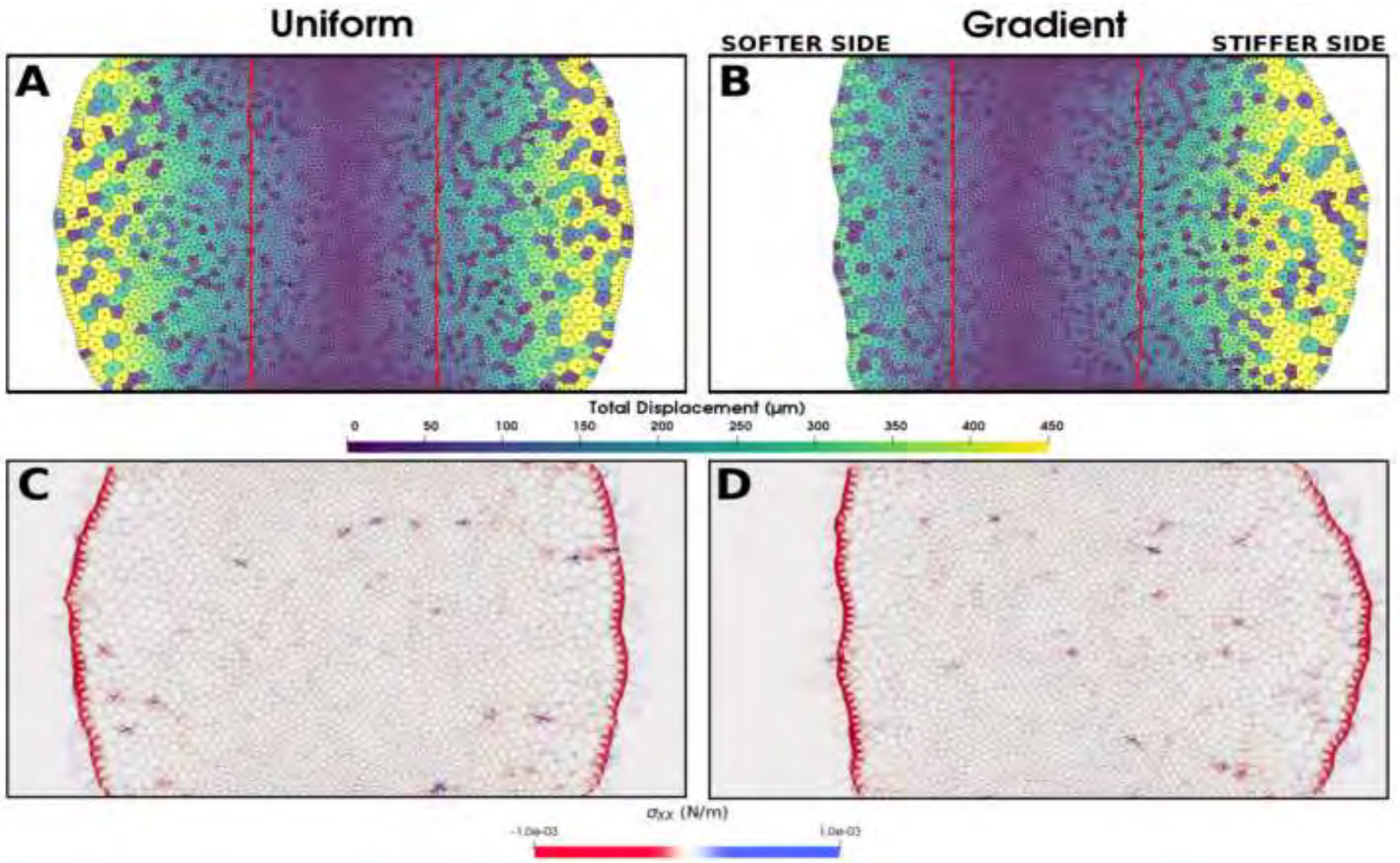

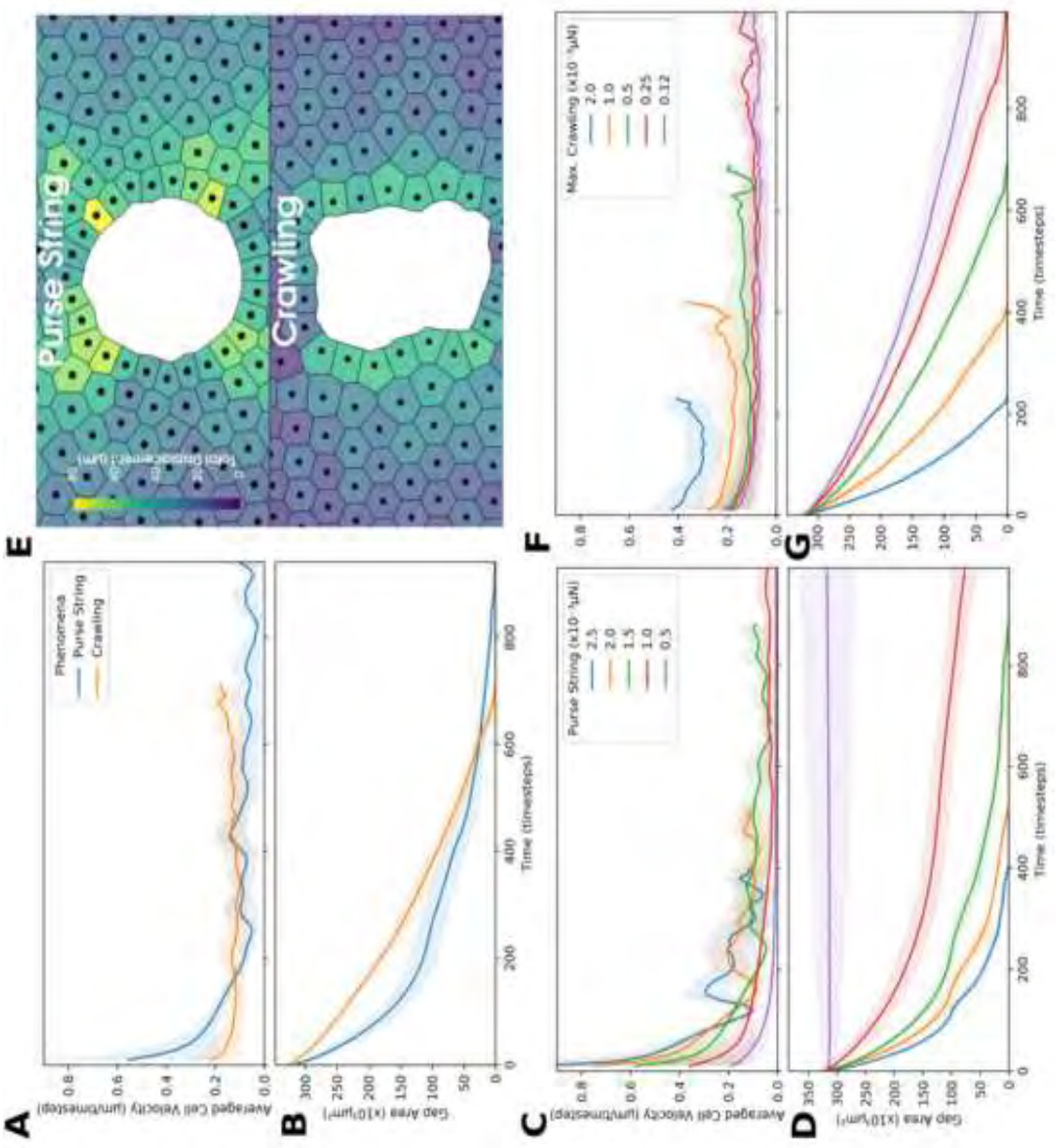

Figure
Click here to download high resolution image

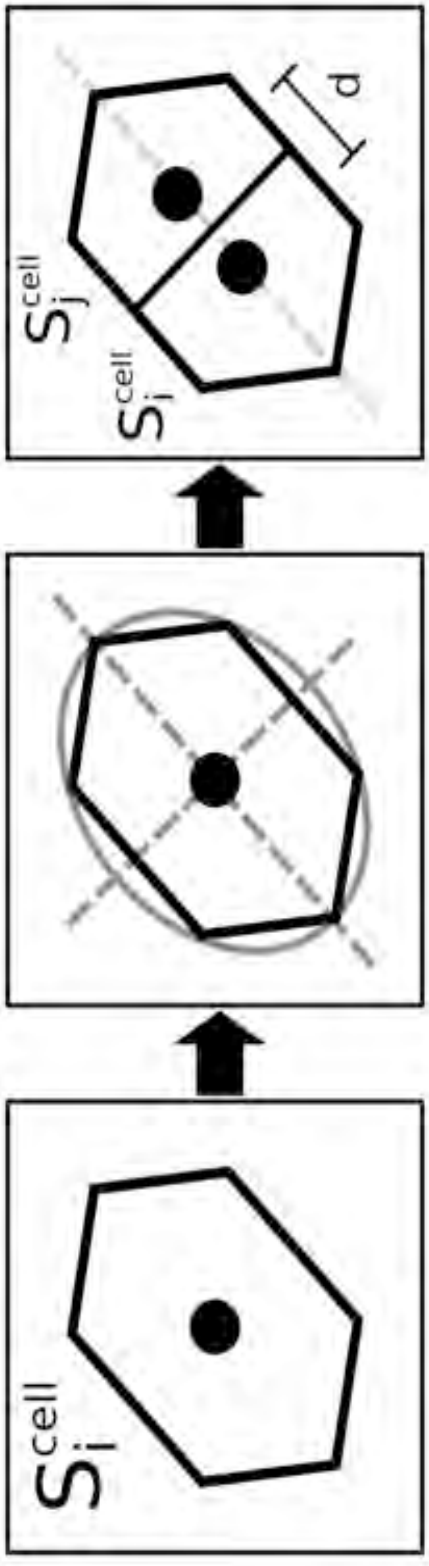

Figure
Click here to download high resolution image

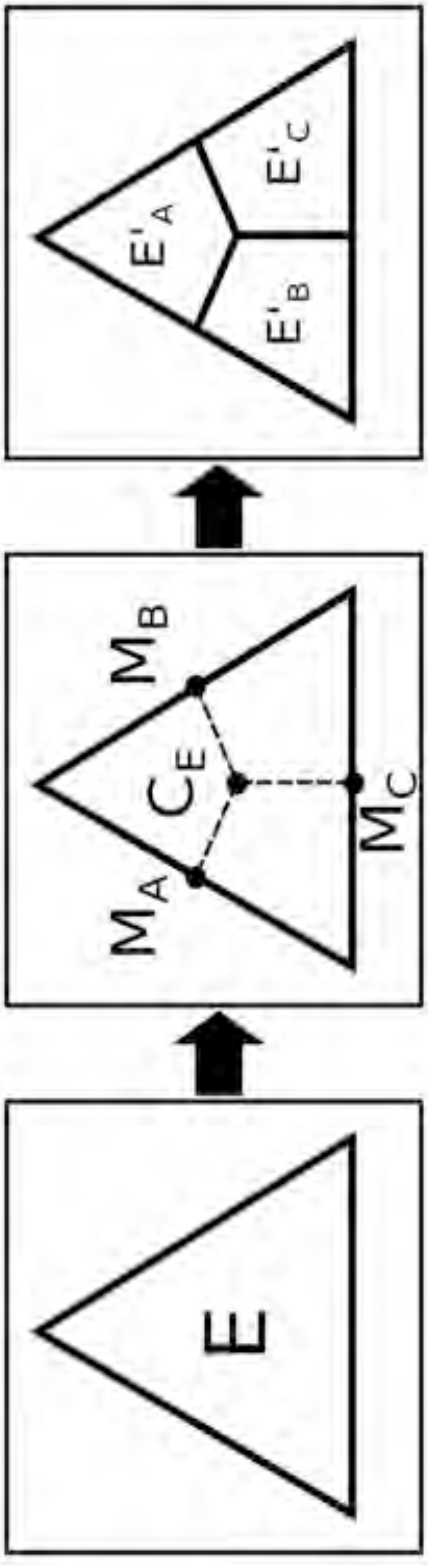

Figure
Click here to download high resolution image

Figure
Click here to download high resolution image